Electrically-functionalised nanoindenter integrated in-situ in a Scanning Electron Microscope : case studies

F Volpi, S Comby-Dassonneville, C Boujrouf, M Rusinowicz, G Parry, M Braccini, S Iruela, A Antoni-Zdziobek, Y Champion, F Charlot, et al.

Electrically-functionalised nanoindenter integrated *in-situ* in a Scanning Electron Microscope : case studies

F. Volpi[a]*, S. Comby-Dassonneville[a], C. Boujrouf[a], M. Rusinowicz[a], G. Parry[a], M. Braccini[a], S. Iruela[a], A. Antoni-Zdziobek[a], Y. Champion[a], F. Charlot[b], R. Martin[b], F. Roussel-Dherbey[b], L. Maniguet[b], J. Fouletier[c], E. Siebert[c], D. Pellerin[d], M. Verdier[a]

[a] Univ. Grenoble Alpes, CNRS Grenoble INP - SIMaP - 38000 Grenoble, France

[b] Univ. Grenoble Alpes, Grenoble INP - CMTC - 38000 Grenoble, France

[c] Univ. Grenoble Alpes, CNRS Grenoble INP - LEPMI - 38000 Grenoble, France

[d] Scientec / CSInstruments - 91940 Les Ulis, France

*Corresponding author : fabien.volpi@grenoble-inp.fr

Abstract

Fundamental understanding and quantitative characterization of electron transport mechanisms between two solids brought into mechanical contact require the development of a dedicated multifunctional device. In this article, we report original measurements and analyses based on a nanoindenter coupled with fine electrical measurements in-situ a Scanning Electron Microscope (SEM). After a description of the experimental set-up, we report quantitative results on resistive-nanoindentation performed on metallic systems with increasing complexity. Starting from a model case (Au single crystal, a noble metal), a procedure is developed, numerically modelled and further applied to a complex rheology structure (200 nm Au thin film plastically deformed against an elastic substrate) to demonstrate the quantitative monitoring of contact area. Then a two-phase AgPdCu alloy is used to illustrate the benefit of local characterisation performed under SEM imaging. The effect of interfacial layer (probably a native oxide film) on the electrical response is discussed. Finally, we present local impedance spectroscopy characterisation of a 10nm-thick alumina layer on aluminium substrate. The conductance through alumina during mechanical compression is discussed in terms of electrochemical processes.

1 Introduction

The understanding and the quantitative analysis of the electro-mechanical processes involved at the interface between two solids are of crucial interest for both academic and applied purposes [1,2]: electric connectors for electrotechnics and automotive applications, intermittent contacts in mechanical switches (at both macro- and micro-scales), microelectronics,... The development of scanning probe microscopy (SPM) triggered the experimental study of these phenomena at small-scale [3,4,5], but only the coupling of electrical measurements with instrumented indentation (independent load and displacement measurements) provided the precise control and monitoring of both contact mechanics and electrical conduction [6]. Initiated by the monitoring of phase transformation under pressure [7,8,9], resistive-indentation has then been extended to the study of other phenomena: native oxide fracture [10,11,12,13], MEMS operation at small scales [14,15] and contact area computation during nanoindentation tests [16,17]. In the past decades, numerous efforts have been made to further expand the capabilities of nanoindentation [6], such as real-time imaging [18,19], coupling with multifunctional characterisation tools [20,21] and high temperature measurements [22].

The present article reports the development and the application of a home-made multifunctional characterisation device based on a commercial nanoindentation head. This device combines mechanical and electrical characterisations, and can be integrated in-situ in a Scanning Electron Microscope (SEM). Quantitative electrical characterisations cover resistive and capacitive measurements (focus is made on resistive measurements in this paper). In-situ SEM integration allows precise positioning of local nanoindentation tests (with a precision better than 100nm) as well as the positioning of electrically-coupled nanoindentation maps. The behaviour of surface oxide layer is also characterised by impedance spectroscopy.

2 Experimental details

The experimental set-up combines different commercial instruments, with customized adapter systems. Fig. 1 presents the Infra-Red view of the set-up once integrated within the SEM chamber.

The nanoindentation head is a commercial actuator (InForce 50 actuator from Nanomechanics Inc / KLA-Tencor), displaying a maximum load of 50mN and a static load resolution below 0.1 µN. This force-controlled actuator enables continuous stiffness measurement (CSM) through locked-in detection of displacements induced by oscillatory loads superimposed to the main load signal. This CSM mode gives access to the continuous extraction of both hardness and elastic modulus during indentation [23]. A fast mapping technique is also available, allowing high-speed nanoindentation tests (~1 indent per second). The indentation tip is screwed on a 1.5 cm-long extension. All the experiments presented in this paper have been performed with boron-doped diamond (BDD) tips with resistivity in the range of [0.2-2] Ω.cm (with either Berkovich, cube-corner or flat-punch shapes). Electrical contacts to the tip are made with thin copper wires connected to fixed sockets. Actuator and sample displacements are performed with linear positioners from SmarAct GmbH. Typical travel ranges are at the cm-scale with a ~1 nm resolution. An overall frame stiffness larger than 10^6 N/m has been extracted, thus validating the overall mechanical behavior.

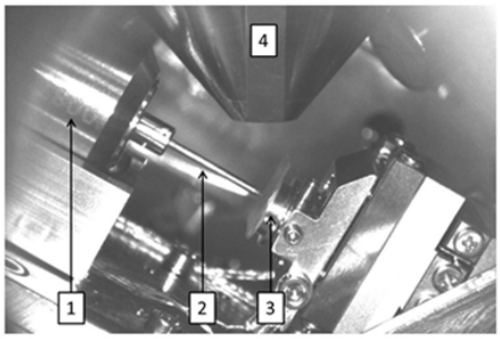

Fig. 1. Infra-Red view of the set-up once integrated within the SEM. (1 = Nanoindenter head, 2 = Extender + tip, 3 = Specimen, 4 = SEM column)

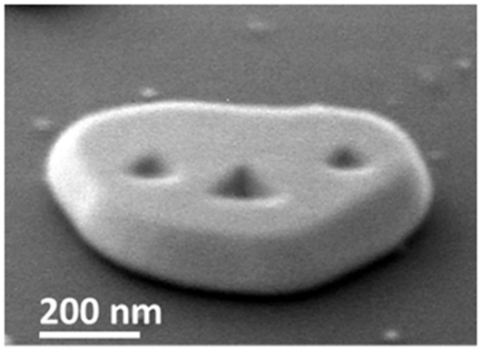

Fig. 2. Illustrations of the set-up performances. Gold crystallites after three individual indents (without tilt-correction).

The SEM apparatus used was a Field Emission Gun (FEG) GEMINI SEM 500 from Zeiss [24]. The arrangement of the analytical tools within the SEM chamber has been optimized to improve the observation angle during indentations. In standard conditions, the specimen surface was scanned under a 60° tilt angle, that was software-corrected during experiments. The SEM-integration allows positioning of indents with a precision better than 100nm. As an illustration, Fig. 2 presents a 0.75µm-large gold island (obtained by dewetting of a gold film on sapphire substrate) after a 'smiley pattern' obtained with three indents.

Resistance measurements were conducted with a ResiScope apparatus from CSI/Scientec. Originally developed for conductive-atomic force microscopy [25], this device is optimised for real-time and self-compliant resistance measurements. It ranges from 100 Ω to 1 TΩ, with acquisition rates up to 1kHz. Impedance spectroscopy measurements were also performed for the characterisation of thin oxide layers: an LCR-meter (Agilent 4980) was used, with a sensitivity better than 1nS for admittance measures at 2MHz.

3 Resistive-nanoindentation of metals

The electrical resistance which is measured during a resistive-nanoindentation test is the sum of several resistances in series (Fig. 3-a): the tip resistance, the interface resistance (oxide, capping layer,…) and the sample resistance. In the case of metallic samples, the latter resistance is negligible. In standard resistive-nanoindentation experiments, the overall resistance tends to decrease as the tip penetrates the sample (Fig. 3-b). This trend is driven by the combination of several mechanisms: (1) as the tip penetrates the sample, the tip-to-sample contact area increases, thus decreasing the overall contact resistance, (2) the interfacial layer (usually insulating) tends to crack, thus allowing direct local tip-to-metal contacts and (3) the spreading resistance through the tip tends to decrease.

3.1 Resistive-nanoindentation on pure metals: effect of a native oxide

The behaviours of three pure metals have been compared: a noble metal (Au) and two natively-oxidised metals (Al and Cu). The two latter were covered with their native-oxide layers characterised by different conduction mechanisms: alumina displays ionic conduction only, while copper oxides display both electronic and ionic conduction. All samples were (111)-oriented bulk single crystals.

A set of resistive-nanoindentation experiments (Resistance-Depth curves) performed with a Berkovich tip under different biases (from 0.5 to 10V) is shown in Fig. 3-b,c,d. On Au, all curves are clearly superimposed, suggesting an ideal ohmic contact (which is confirmed by current-voltage characteristics, not shown here). This behaviour will be quantitatively

analysed in Part 3.2. On the contrary, the two oxidised metals display drastically different behaviours: much larger resistances are measured (up to 6 orders of magnitude larger with aluminum) and highly-non-linear behaviour is observed. The lower dispersion observed on copper (compared to aluminum) is a signature of the electronic conductivity in copper-oxides, while oxido-reduction reactions are supposed to be the cause of the highly-dispersed data on aluminum (discussed in Part 3.4).

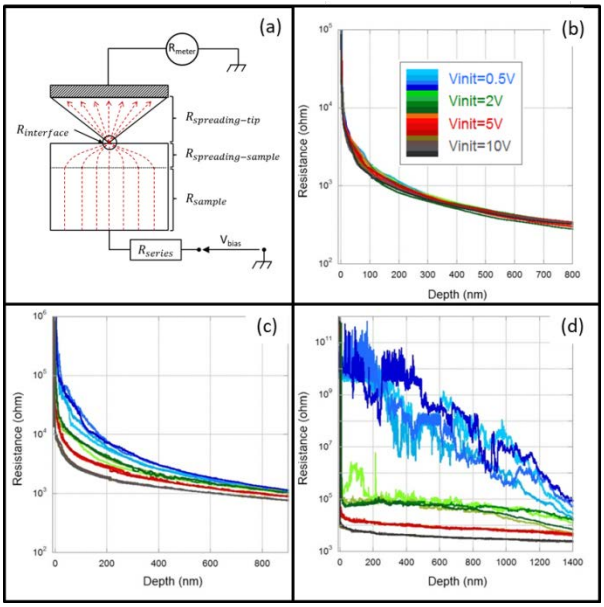

Fig. 3. Resistive-nanoindentation illustrations. (a) Schematic of the resistance contributions. Set of resistive-nanoindentation tests on Au (b), Cu (c) and Al (d).

3.2 Resistive-nanoindentation on noble metals

3.2.1 Experiments

In the case of noble metals, the absence of interfacial layer leads to measure the tip resistance only (Fig. 4-a). Under this condition, the measured resistance can be simply given by (1) (for more details, see [26]):

$$R_{measured} = A + B/(h_c+h_0) \quad (1)$$

A and B are two constants that depend only on the experimental set-up (tip geometry and resistivity, series resistance,…) but not on the specimen (A and B have to be determined experimentally during the calibration step, see below). h_0 is the length of the tip defect (unavoidable rounded apex of the tip). Even though expression (1) relies on strong approximations (self-similar shape of the tip, homogeneous distribution of current lines through the contact,…), it is verified experimentally (Fig. 4). In order to validate this approach, a finite element (FE) modelling of this experiment was carried out.

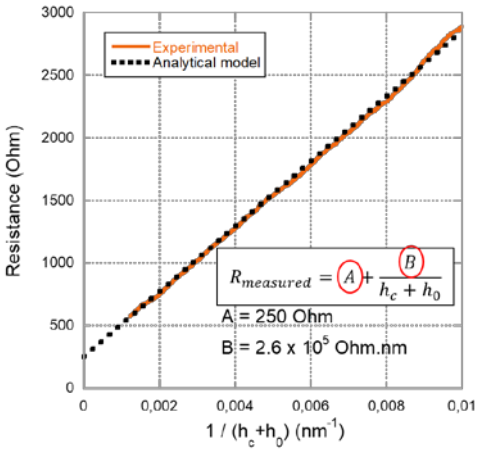

Fig. 4. Linear fitting of resistive-nanoindentation data according to Equation 1.

3.2.2 Finite-Element Modelling

FE modelling was performed in 2D axisymmetric (Fig. 5-a). The commercial FE software ABAQUS®/Standard was used. The indenter was a Berkovich tip defined as an elastic body and built from an experimental area function (fused silica reference sample using Oliver and Pharr method). The sample (Au) was defined as an elasto-plastic cylinder with a 10µm radius and height. The mechanical behavior of Au was modeled by a Hooke's law for the elastic part (E = 77.2GPa ; ν = 0.42) and by a Hollomon power law for the plastic part which has the following form:

$$\sigma_{Plastic} = K\epsilon_{plastic}^{n} \quad (2)$$

where K and n are constants which were used as fitting parameters in order to reproduce the experimental Load-Depth curves (see Tab. 1).

Concerning the electrical coupling, the electrical conduction in the tip and in the sample was modeled using a pure ohmic law with an electrical conductivity extracted from previous works [27].

The two parts were meshed with axisymmetric deformation element CAX3T. Frictionless mechanical contact was defined by default. During loading, a displacement of 1µm along the vertical direction z was applied to the top surface of the tip. For the electrical boundary conditions, a 10V bias was applied between the top surface of the tip (0V) and the bottom surface of the sample (10V). Post treatment using a Python subroutine made it possible to extract load, penetration depth, contact depth, contact area and electrical resistance.

Without any advanced fitting process, the FE-modelled Resistance-Depth curves show remarkable match with the experimental data (Fig. 5-b). And the linear dependence of resistance with the reciprocal of the contact depth (Equation 1) is numerically confirmed (Fig. 5-c). This is explained by the homothetic distribution of current lines through the contact interface at the periphery of the contact [26].

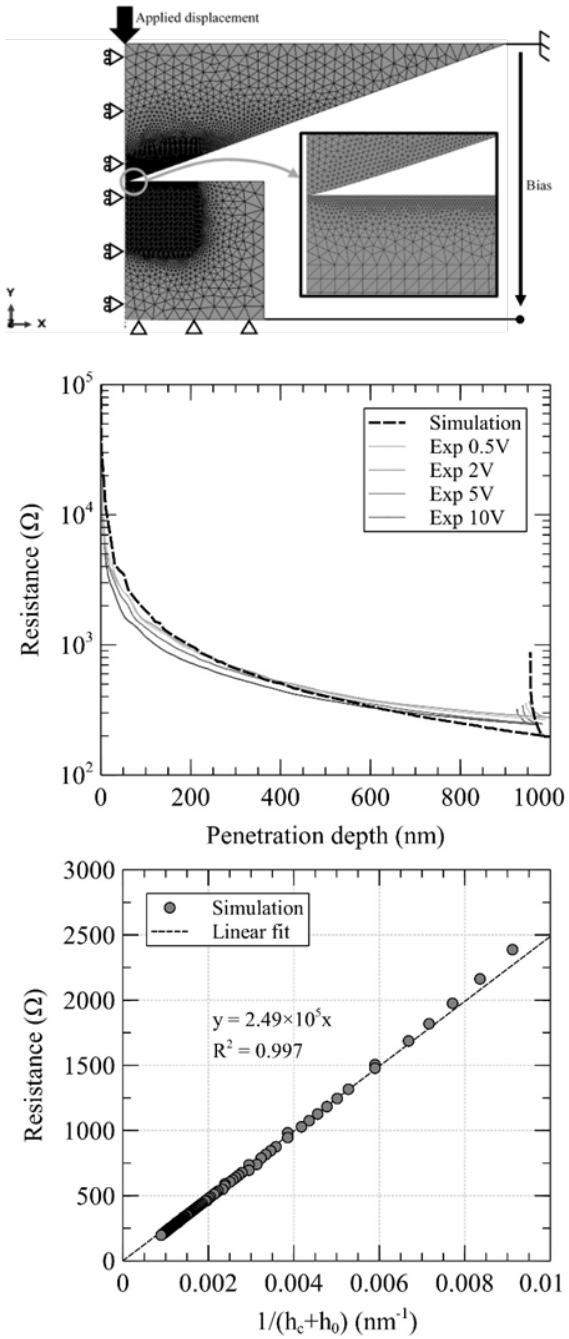

Fig. 5. Numerical modelling. (a) System model. (b) Comparison of simulated and experimental resistive-nanoindentation tests. (c) Linear fitting of simulated resistive-nanoindentation data.

Tab. 1. Parameters of the Hollomon law describing the plastic behaviour of bulk gold, fitted to the experimental data.

Parameter	σ_y	K	n
Value	100 MPa	230 MPa	0.1

3.2.3 Application to the real-time monitoring of contact area

The real-time monitoring of resistance during nanoindentation is of particular interest for the quantitative analysis of nanoindentation tests. Indeed, the simultaneous computation of sample Young's modulus and hardness relies on a precise knowledge of the contact area A_c. However even for the simplest cases of homogeneous semi-infinite specimens, the determination of A_c is strongly affected by pile-up or sink-in phenomena that occur at the contact periphery (Fig. 6). The actual contact area may then be misinterpreted by 20-30%. The standard methods widely used to extract contact area require analytical models based on material rheology assumptions [28,29]. On the contrary, the direct monitoring of contact area by resistive-nanoindentation should bring supplementary inputs for the quantitative analysis of indentation tests. Some attempts to combine micro- or nano-indentation to resistive measurements to quantitatively analyse the indentation process have been reported [16,17] but the monitoring of contact area was not processed.

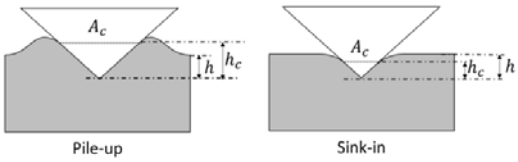

Fig. 6. Effect of material rheology on contact area and contact depth. The penetration depth h is the depth reached by the tip from the initial specimen surface, while the contact depth h_c describes the contact height of the tip with the specimen.

One of the bottleneck steps for the quantitative analysis of resistive-nanoindentation tests is the appropriate analytical description of the electrical measurement chain.

This description being established, the experimental extraction of the contact area can be processed through a 3-step procedure:

- Step 1: The tip geometry is determined from direct AFM characterisation. This step generates the tip "shape function" that relates the projected contact area to the contact depth h_c.
- Step 2: An electrical calibration is carried out (on a gold bulk single crystal for instance), aiming at the determination of the A and B constants (see (1)). As A and B depend only on the experimental set-up, a one-to-one analytical correspondence is then established between the electrical resistance and the contact depth (independently of the specimen).
- Step 3: The contact area monitoring of any oxide-free specimen can then be performed. Using the tip shape function (step 1), the contact area is finally determined from the contact depth values (step 2) for this specimen to be characterized.

This procedure has been applied and validated on a 200 nm-thick polycrystalline gold film deposited on a sapphire substrate. Such a composite geometry is a model case of complex rheology which is depth-dependent and where no analytical model exists. To do so, resistive-nanoindentation tests with various final penetration depths have been performed. For each test, post-mortem AFM measurements have been conducted to compare the contact area to the one monitored by our procedure. Fig. 7 shows an excellent agreement between our predictions and the effective areas. For comparison, the contact area computed from the standard Oliver-Pharr method [28] (based on sink-in assumption) is also reported showing a ~50% discrepancy. Such a precise monitoring of the tip-to-sample contact area has been reported for the first time in literature in [26].

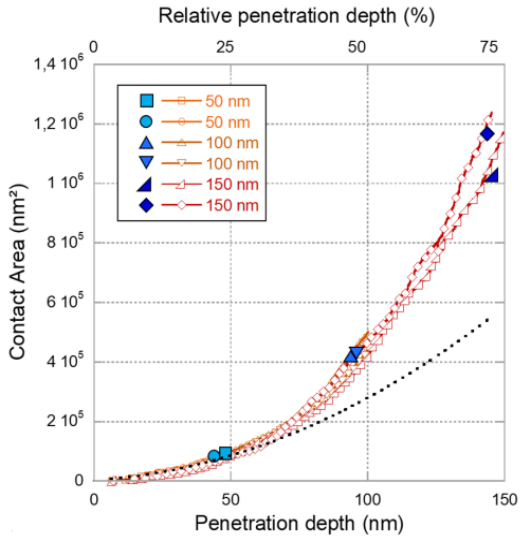

Fig. 7. Contact area against penetration depth on the Au thin film. Comparison of the computed data (open markers) with the corresponding post-mortem AFM measurements (solid markers). Predicted contact area from Oliver and Pharr model in dotted line.

3.3 Resistive-nanoindentation of multi-phased alloys

As already mentioned, the integration of this resistive-nanoindentation set-up within the SEM allows precise positioning of the spot to analyze as well as the electro-mechanical mapping of a specimen surface. These two advantages are illustrated through the study of an AgPdCu alloy designed to combine high conductivity and large yield strength. Fig. 8 presents an SEM view of the sample after a local indent performed on the Ag-rich phase (lightest contrast in the SEM image). The darkest domain is constituted of Cu-rich phases.

Fig. 9 (a)-(b) collect the resistance and hardness measurements obtained over 28 indents on the two domains. These electrical and mechanical data clearly discriminate the Ag- and Cu-rich phases. The Cu-rich domain appears as more conductive than the Ag-rich one, but it also appears as harder. The higher resistance of the Ag-rich domain can be attributed either to a larger intrinsic resistivity, to a more resistive native-oxide or to different material rheologies.

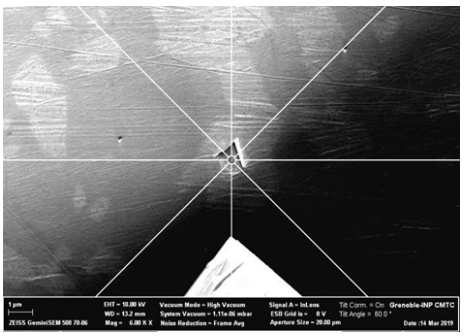

Fig. 8. SEM view of an indent left after local testing of the Ag-rich phase. The white triangle at the bottom of the image is the indenter tip.

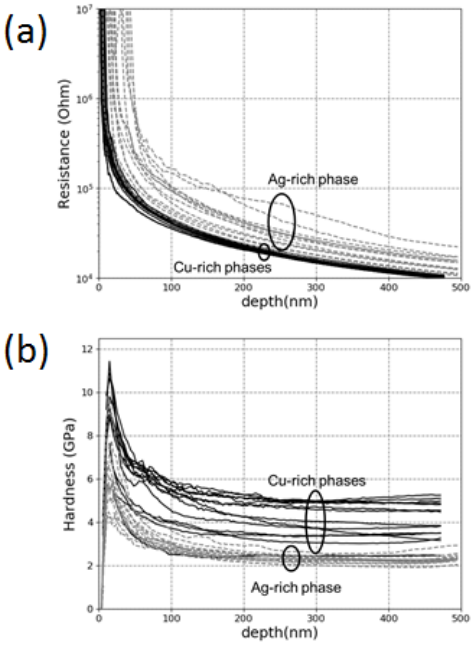

Fig. 9. Electrical and mechanical data from 28 indents performed in both Ag- and Cu-rich phases. (a) Resistance and (b) Hardness evolutions with indentation depth. Hardness data were extracted from Oliver-Pharr model [26].

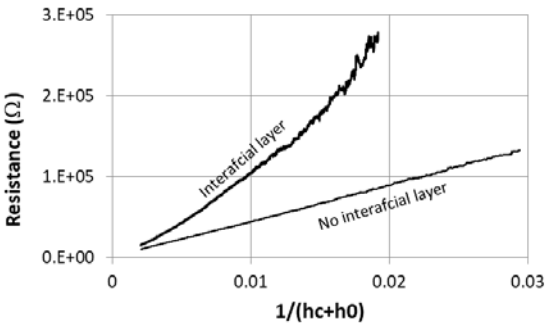

Fig. 10. Evolution of resistance against $1/(h_c+h_0)$ on two distinct indents.

The plotting of resistance against $1/(h_c+h_0)$ (according to Equation 1) is shown in Fig. 10. It clearly discriminates the ideal indents (linear dependence) from those affected by an interfacial layer (non-linear dependence), most-likely an oxide layer. This behaviour supports the need for a deeper analysis of oxide-covered metals.

3.4 Resistive-nanoindentation of oxide-covered metals

In the case of oxidised metals, the electrical resistance is essentially controlled by the conduction mechanisms through the oxide layer. A set of experiments have been performed on a 10nm thick alumina film deposited by Atomic Layer Deposition onto an aluminum substrate.

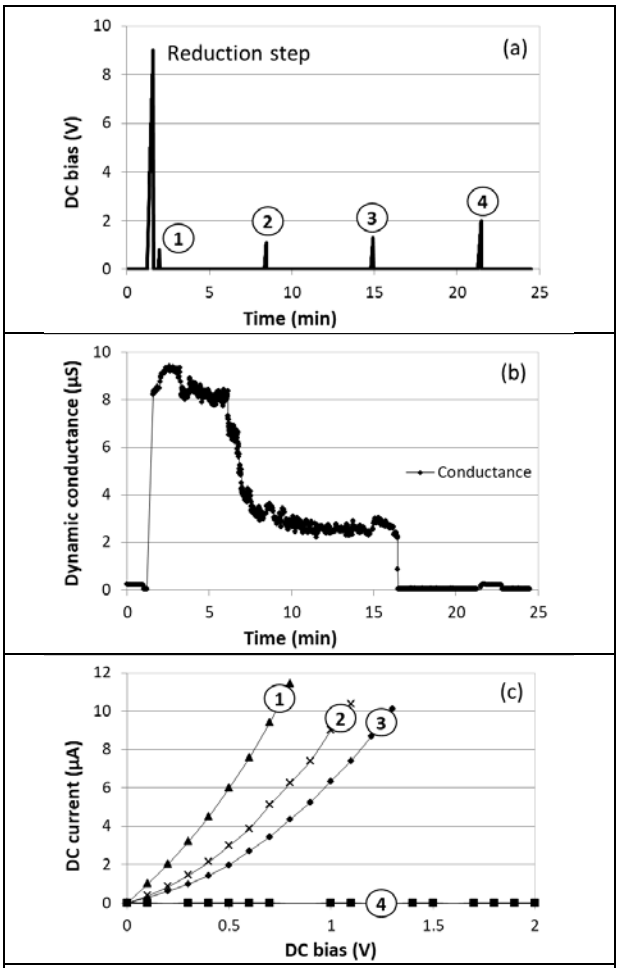

Fig. 11. Characterisation of a 10nm-thick alumina film (under mineral oil). (a) Timeline of the test protocol. (b) Evolution of the dynamic conductance during test. (c) Current-Voltage characteristics during alumina recovery.

For these experiments, compression tests were performed with a 5µm large flat-punch tip. The tip was set into contact with the alumina surface with a low load (100 µN, leading to an applied stress close to 5 MPa). Once the contact set, impedance-spectroscopy measurements were performed with an LCR-meter. The experiment timeline was the following (Fig. 11-a): a large voltage scan (referred as "Reduction step") was first applied in order to reduce locally the alumina film, then dynamic conductance and capacitance were monitored continuously, while small voltage scans were performed every 5 min to monitor the alumina recovery (voltage scans 1 to 4).

After the "Reduction step", the conductance is seen to increase drastically (Fig. 11-b). This "Reduction step" most likely corresponds to the reduction of oxygen vacancies according to the following reaction (formation of F-centres):

$$V_O^{oo} + e' \rightarrow V_O^o$$

At this point, the alumina layer becomes conductive, and its conductance remains high for more than 15 min (up to 1h for some tests). The four current-voltage scans (Fig. 11-c) clearly confirm the decrease of DC-conductance, and the final recovery of alumina insulation (scan 4).

The same experiments were performed with the surface immersed into a mineral oil drop (to limit any interaction with atmospheric oxygen). Since similar results were obtained, it is concluded that atmospheric oxygen is not responsible for the final re-oxidation of F-centres.

Numerical simulations are in progress in order to describe the mechanical and electrical behaviour of this alumina layer under mechanical stress. Fig. 12 reports exploratory results, where high radial tensile stresses are identified at the tip apex and periphery (see inserts).

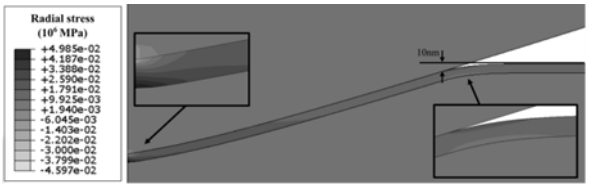

Fig. 12. Numerical modelling of an alumina/aluminum stack under resistive-nanoindentation testing.

4 Conclusion

An experimental set-up dedicated to the coupling of local electrical and mechanical characterisations is presented. This set-up combines a nanoindentation head to fine electrical measurements *in-situ* in a scanning electron microscope. The ability of the set-up to characterise the contact with oxide-free or oxidized metals is shown. First the ability to monitor quantitatively the contact area all along a nanoindentation test is demonstrated. Then a two-phase metallic system is characterized through individual local indents. Finally the electrical behaviour of an oxide layer is analysed and described on the basis of electrochemical processes. Numerical modelling of the experiments is

used to support the understanding of the overall system behaviour.

5 Acknowledgment

This work has been performed with the financial support of the Centre of Excellence of Multifunctional Architectured Materials "CEMAM" n° ANR-10-LABX-44-01. The CEMAM program is funded by the French Agence Nationale de la Recherche (ANR).
The authors thank the technical team of SIMaP lab (B. Mallery, S. Massucci, N. Vidal) for its support, the CMTC platform (physico-chemical characterization platform of Grenoble INP), as well as members of CSI/Scientec company (Les Ulis, France) for their support for the functionalization of the nanoindentation head: L. Pacheco, A. Lecoguiec and S. Poulet.

5 Literature

[1] R. Holm. “Electrics Contacts, Theory and Applications”, Springer, 2000.
[2] M. Braunovic, V.V. Konchits, N.K. Myshkin, “Electrical Contacts, Fundamental, Applications and Technology” , “BRAU”, CRC Press, 2007.
[3] G. Binnig, C. F. Quate, and Ch. Gerber, “Atomic Force Microscope”, Phys. Rev. Lett. 56, 930, 1986.
[4] W. Vandervorst, M.Meuris, European patent 466274, 1992
[5] P.Eyben, W.Vandervorst, D.Alvarez, M.Xu, and M.Fouchier, “Probing Semiconducteurs Technology and Devices with Scanning Spreading Resistance Microscopy”, in “Scanning Probe Microscopy Electrical and Electromechanical Phenomena at the Na Probing”, Springer, 2007.
[6] H. Nili, K. Kalantar-Zadeh, M. Bhaskaran, S. Sriram, “In situ nanoindentation: Probing nanoscale multifunctionality”, Prog Mater Sci. 58, 2013.
[7] D. R. Clarke, M. Kroll, P. D. Kirchner, R. F. Cook, B. J. Hockey, “Amorphization and Conductivity of Silicon and Germanium Induced by Indentation” Phys. Rev. Lett. 60 2156-2159, 1988.
[8] G. M. Pharr, W. C. Oliver, R. F. Cook, P. D. Kirchner, M. Kroll, T. R. Dinger, “Electrical resistance of metallic contacts on silicon and germanium during indentation”, J. Mater. Res. 7 961-972, 1992.
[9] S. Ruffell, J. E. Bradby, J. S. Williams, O. L. Warren, “An in situ electrical measurement technique via a conducting diamond tip for nanoindentation in silicon”, J. Mater. Res. 22 578-585, 2007.
[10] J. B. Pethica, D. Tabor, “Contact of characterised metal surfaces at very low loads: Deformation and adhesion”, Surf. Sci. 89 189-190, 1979.
[11] D. D. Stauffer, R. C. Major, D. Vodnick, J. H. Thomas, J. Parkern, M. Manno, C. Leighton, W. W. Gerberich, “Plastic response of the native oxide on Cr and Al thin films from in situ conductive nanoindentation”, J. Mater. Res. 27 685-693, 2012.
[12] H. H. Nguyen, P. J. Wei, J. F. Lin, “Electric contact resistance for monitoring nanoindentation-induced delamination”, Adv. Nat. Sci.: Nanosci. Nanotechnol. 2 015007-1-4, 2011.
[13] T. Shimizu, T. Horie, N. Watanabe, J. Miyawaki, S. Fujii, Y. Yamagata, T. Kondo, M. Onuma, “The investigation of electrical contacts using newly designed nano-indentation manipulator in scanning electron microscope”, Proc. 60th IEEE Holm Conf. Elect. Cont. 403-406, 2014.
[14] P. Y. Duvivier, V. Mandrillon, K. Inal, C. Dieppedale, S. Deldon-Martoscia, J. P. Polizzi, “Investigation of the Electrical Resistance of Au / Au Thin Film Micro Contacts”, Proc. 56th IEEE Holm Conf. Elect. Cont. 58-64 Time Dependence, 2010.
[15] B. Arrazat, P. Y. Duvivier, V. Mandrillon, K. Inal, “Discrete Analysis of Gold Surface Asperities Deformation under Spherical Nano-Indentation Towards Electrical Contact Resistance Calculation”, Proc. 57th IEEE Holm Conf. Elect. Cont.1-8, 2011.
[16] L. Fang, C. L. Muhlstein, J. G. Collins, A. L. Romasco, L. H. Friedman, “Continuous electrical in situ contact area measurement during instrumented indentation”, J. Mater. Res. 23 2480-2485, 2008.
[17] D. J. Sprouster, S. Ruffel, J. E. Bradby, D. D. Stauffer, R. C. Major, O. L. Warren, J. S. Williams, “Quantitative electromechanical characterization of materials using conductive ceramic tips”, Acta Mater. 71 153-163, 2014.
[18] Rabe R, Breguet JM, Schwaller P, Stauss S, Haug FJ, Patscheider J, et al, “Observation of fracture and plastic deformation during indentation and scratching inside the scanning electron microscope”, Thin Solid Films, 469–470:206–13, 2004.
[19] Wall MA, Dahmen U, “Development on an in situ nanoindentation specimen holder for the high voltage electron microscope”, Microsc Microanal ; 3:593–4, 1997.
[20] Sridhar S, Giannakopoulos AE, Suresh S, Ramamurty U. “Electrical response during indentation of piezoelectric materials: a new method for material characterization”, J Appl Phys, 85:380–7, 1999.
[21] Rar A, Pharr GM, Oliver WC, Karapetian E, Kalinin SV. “Piezoelectric nanoindentation”, J Mater Res ;21:552–6, 2006.

[22] Schuh CA, Packard CE, Lund AC. “Nanoindentation and contact-mode imaging at high temperatures”, J Mater Res; 21:725–36, 2006.
[23] W. C. Oliver and G. M. Pharr, “Measurement of hardness and elastic modulus by instrumented indentation: Advances in understanding and refinements to methodology”, J. Mater. Res., Vol. 19, No. 1, Jan 2004.
[24] L. Maniguet, F.Roussel, R.Martin, E.Djurado, M.C.steil, E.Bichaud, A.LeGo, M. Holzinger, S.Cosnier, J.M.Chaix, and C.Carry, “Fuel cells and ceramic-characterizing real-worlds sample with a fesem ready for challenges”, Microscopy and Analysis, 21:47, 2015.
[25] F. Houzé, R.Meyer, O.Schneegans, and L.Boyer, “Imaging the local electrical properties of metal surfaces by atomic force microscopy with conducting probes”, Applied Physics Letters, 69:19751977, 1996.
[26] S.Comby-Dassonneville, F. Volpi, G. Parry, D. Pellerin, M. Verdier, “Resistive-nanoindentation: contact area monitoring by real-time electrical contact resistance measurement”, MRS Communications, Vol. 9 (3), 1008-1014, 2019
[27] https://tel.archives-ouvertes.fr/tel-01897366
[28] W. C. Oliver, G. M. Pharr, “An improved technique for determining hardness and elastic modulus using load and displacement sensing indentation experiments”, J. Mater. Res.7 1564-1582, 1992.
[29] J. L. Loubet, M. Bauer, A. Tonck, S. Bec, B. Gauthier-Manuel, “Mechanical Properties and Deformation Behavior of Materials Having Ultra-Fine Microstructures : Nanoexperiments with a surface force apparatus”, in: M. Nastasi, D. M. Parkin, H. Gleiter (Eds.), “Mechanical Properties and Deformation Behavior of Materials Having Ultra-Fine Microstructures”, Kluwer Academic Publisher 429-447, 1993